A Spitzer-selected Galaxy Cluster at z = 1.62

Papovich, C ; Momcheva, I ; Willmer, C N A ; et al ; Tran, K-V

Abstract: We report the discovery of a galaxy cluster at z = 1.62 located in the Spitzer Wide-Area Infrared Extragalactic survey XMM-LSS field. This structure was selected solely as an overdensity of galaxies with red Spitzer/Infrared Array Camera colors, satisfying ([3.6] - [4.5])AB> - 0.1 mag. Photometric redshifts derived from the Subaru XMM Deep Survey (BViz bands), the UKIRT Infrared Deep Survey-Ultra-Deep Survey (UKIDSS-UDS, JK bands), and from the Spitzer Public UDS survey (3.6-8.0 m) show that this cluster corresponds to a surface density of galaxies at z 1.6 that is >20 above the mean at this redshift. We obtained optical spectroscopic observations of galaxies in the cluster region using IMACS on the Magellan telescope. We measured redshifts for seven galaxies in the range z = 1.62-1.63 within 2.8 arcmin (<1.4 Mpc) of the astrometric center of the cluster. A posteriori analysis of the XMM data in this field reveal a weak (4) detection in the [0.5-2 keV] band compatible with the expected thermal emission from such a cluster. The color-magnitude diagram of the galaxies in this cluster shows a prominent red sequence, dominated by a population of red galaxies with (z - J)>1.7 mag. The photometric-redshift probability distributions for the red galaxies are strongly peaked at z = 1.62, coincident with the spectroscopically confirmed galaxies. The rest-frame (U - B) color and scatter of galaxies on the red sequence are consistent with a mean luminosity-weighted age of 1.2 ± 0.1 Gyr, yielding a formation redshift $\overline{z\_f} = 2.35 \pm 0.10$, $and correspondingtothelastsignificantstarformationperiodinthesegalaxies.Thisworkisbasedinpartonobservation$

DOI: https://doi.org/10.1088/0004-637X/716/2/1503

SUBMITTED TO THE ASTROPHYSICAL JOURNAL
Preprint typeset using LaTeX style emulateapj v. 11/10/09

A SPITZER–SELECTED GALAXY CLUSTER AT Z=1.62[1]

C. PAPOVICH[2], I. MOMCHEVA[3], C. N. A. WILLMER[4], K. D. FINKELSTEIN[2], S. L. FINKELSTEIN[2], K.–V. TRAN[2], M. BRODWIN[5], J. S. DUNLOP[6], D. FARRAH[7], S. A. KHAN[8,9], J. LOTZ[10], P. MCCARTHY[3], R. J. MCLURE[6], M. RIEKE[4], G. RUDNICK[11] AND S. SIVANANDAM[4]

Submitted to the Astrophysical Journal

ABSTRACT

We report the discovery of a galaxy cluster at z=1.62 located in the *Spitzer* Wide-Area Infrared Extragalactic survey XMM-LSS field. This structure was selected solely as an overdensity of galaxies with red *Spitzer*/IRAC colors, satisfying $([3.6]-[4.5])_{\rm AB} > -0.1$ mag. Photometric redshifts derived from Subaru XMM Deep Survey (*BViz*-bands), UKIRT Infrared Deep Survey–Ultra-Deep Survey (UKIDSS-UDS, *JK*-bands), and from the *Spitzer* Public UDS survey (3.6-8.0 micron) show that this cluster corresponds to a surface density of galaxies at $z \approx 1.6$ that is $> 20\sigma$ above the mean at this redshift. We obtained optical spectroscopic observations of galaxies in the cluster region using IMACS on the Magellan telescope. We measured redshifts for seven galaxies in the range z=1.62–1.63 within 2.8 arcmin (< 1.4 Mpc) of the astrometric center of the cluster. The color–magnitude diagram of the galaxies in this cluster shows a strong red-sequence, dominated by a population of red galaxies with $(z-J) > 1.7$ mag. The photometric redshift distributions for the red galaxies are strongly peaked at $z = 1.62$, coincident with the spectroscopically confirmed galaxies. The rest–frame $(U-B)_0$ color and scatter of galaxies on the red-sequence are consistent with a mean luminosity–weighted age of 1.2 ± 0.1 Gyr, corresponding to a formation redshift $\overline{z_f} = 2.40 \pm 0.15$, and implying that most of the stellar mass in this cluster formed during that period.

Subject headings: large-scale structure of the universe — galaxies: clusters: general — galaxies: clusters: individual (XMM-LSS 02182-05102) — galaxies: evolution

1. INTRODUCTION

Galaxy clusters provide important samples to study both the evolution of large–scale structure and the formation of galaxies. The evolution of the number density of massive galaxy clusters involves only gravitational physics, and thus depends only on the cosmic mass density and initial power spectrum of density fluctuations (e.g., Eke et al. 1998; Bahcall et al. 1999; Borgani et al. 2001; Haiman et al. 2001; Springel et al. 2005). Because the massive galaxies in clusters formed nearly contemporaneously at $z \gg 1$ with similar star–formation and assembly histories (e.g., Stanford et al. 1998; Tran et al. 2007; Eisenhardt et al. 2008), observations of the evolution of distant cluster galaxies provide strong constraints on hierarchical galaxy evolution models, which make detailed predictions for the formation of these objects (e.g., De Lucia & Blaizot 2007).

Studies of high–redshift clusters have been frustrated by small sample sizes. Few clusters have confirmed redshifts beyond $z \sim 1.3$ (e.g., Mullis et al. 2005; Stanford et al. 2005; Brodwin et al. 2006; Stanford et al. 2006; Eisenhardt et al. 2008; Kurk et al. 2009; Wilson et al. 2009). This dearth of detected galaxy clusters at $z > 1.3$ stems from the significant challenges and potential biases in identifying these structures. Deep X–ray surveys have identified spectroscopically confirmed clusters to $z \lesssim 1.5$ (e.g., Rosati et al. 2004; Stanford et al. 2006), but these typically require relaxed systems, which is unlikely to be the case at high redshifts where cluster progenitors will be less massive and more disordered, with less time for the intracluster medium to thermalize (e.g., Rosati et al. 2002). Searches for galaxy overdensities around distant radio galaxies require the presence of a massive central galaxy (e.g., Kurk et al. 2000; Miley et al. 2004; Stern et al. 2003; Kodama et al. 2007; Venemans et al. 2007; Zirm et al. 2008; Chiaberge et al. 2010), which may not be an intrinsic property of cluster progenitors.

Other searches utilize the empirically observed, tight color–magnitude relation in central cluster galaxies (the "red sequence", e.g., Visvanathan & Sandage 1977; Gladders & Yee 2005; Gladders et al. 2007; Kajisawa et al. 2006; Muzzin et al. 2009). However, this selection is biased potentially against clusters whose galaxies have had recent star formation (and overdensities of blue, star–forming galaxies at high redshift have been identified, e.g., Steidel et al. 2005). Most studies of cluster galaxies imply their stellar populations formed at $z_f \gtrsim 1.5$ (e.g.,

[1] This work is based in part on observations made with the Spitzer Space Telescope, which is operated by the Jet Propulsion laboratory, California Institute of Technology, under NASA contract 1407. This paper also includes data gathered with the 6.5 meter Magellan Telescopes located at Las Campanas Observatory, Chile. This work is based in part on data collected at Subaru Telescope, which is operated by the National Astronomical Observatory of Japan.

[2] George P. and Cynthia Woods Mitchell Institute for Fundamental Physics and Astronomy, and Department of Physics and Astronomy, Texas A&M University, College Station, TX, 77843-4242; papovich@physics.tamu.edu

[3] Observatories, Carnegie Institution of Washington, 813 Santa Barbara St., Pasadena, CA, 91101

[4] Steward Observatory, University of Arizona, 933 N. Cherry Ave., Tucson, AZ 85721

[5] W. M. Keck Postdoctoral Fellow, Harvard–Smithsonian Center for Astrophysics, 60 Garden St., Cambridge, MA 02138

[6] Institute for Astronomy, Royal Observatory, University of Edinburgh, UK

[7] Astronomy Centre, University of Sussex, Falmer, Brighton, UK

[8] Pontificia Universidad Católica, Departamento de Astronomía y Astrofísica, 4860 Av. Vicuña Mackenna, Casilla 306, Santiago 22 Chile

[9] Shanghai Key Lab for Astrophysics, Shanghai Normal University, Shanghai 200234, China

[10] Leo Goldberg Fellow, National Optical Astronomy Observatories, 950 N. Cherry Ave., Tucson, AZ 85719

[11] Department of Physics and Astronomy, University of Kansas, 1251 Wescoe Hall Dr., Lawrence, KS, 66045-7582

van Dokkum & van der Marel 2007), concurrent with the peak epoch in the star–formation rate density from UV and IR measurements (see e.g., Hopkins & Beacom 2006). As searches for clusters approach the redshift of their formation, cluster galaxies should show increasing indications for star formation with less time available to build up a substantial red–sequence population.

We have initiated a search for galaxy cluster candidates at $z > 1.3$ selected solely as overdensities of galaxies with red [3.6]−[4.5] colors using data from the Infrared Array Camera (IRAC) on board *Spitzer* (Papovich 2008).[12] At $z<1$ model stellar populations have blue [3.6]−[4.5] colors because these bands probe the stellar Rayleigh–Jeans tail. At $z\gtrsim1$ both star–forming and passively evolving stellar populations appear red in [3.6]−[4.5] as these bands probe the peak of the stellar emission at 1.6 μm (see Simpson & Eisenhardt 1999; Sawicki 2002; Papovich 2008). Therefore, selecting overdensities of red [3.6]−[4.5] sources potentially identifies high–redshift cluster candidates with little bias from galaxy stellar populations. Papovich (2008) showed that IRAC–selected $z > 1.3$ cluster candidates from the *Spitzer* Wide–Infrared Extragalactic (SWIRE) survey have clustering scale lengths of $r_0 \approx 20\ h^{-1}$ Mpc, consistent with other high–redshift galaxy clusters (see Brodwin et al. 2007).

Here we report the discovery and spectroscopic confirmation of a galaxy cluster, XMM–LSS J02182-05102, hereafter designated IRC 0218–A (*Infrared Cluster* "A" in the 0218-051 field from the catalog of Papovich 2008), and we discuss its photometric and spectroscopic properties. This galaxy cluster was identified using our IRAC color selection with no other additional criteria imposed. In § 2 we discuss the target selection, and photometric and spectroscopic observations. In § 3 we present the evidence supporting the assertion that this structure is a galaxy cluster, and in § 4 we discuss its properties. In § 5 we summarize our results. Unless otherwise noted we report all magnitudes in reference to the Johnson (1966) magnitude system relative to Vega. We explicitly denote magnitudes relative to the absolute bolometric system (Oke & Gunn 1983) with an AB subscript, $m_{\rm AB} = 23.9 - 2.5\log(f_\nu/1\,\mu{\rm Jy})$. We use cosmological parameters $\Omega_m = 0.3$, $\Lambda = 0.7$, and $H = 70$ km s^{-1} Mpc^{-1} throughout. For this cosmology, the angular diameter distance is 0.5 Mpc arcmin^{-1} at $z = 1.62$.

2. SAMPLE SELECTION AND SPECTROSCOPIC OBSERVATIONS

2.1. *Identification of High–redshift Galaxy Cluster Candidates*

We identified galaxy cluster candidates at $z \gtrsim 1.3$ using the IRAC data from the SWIRE survey. This data cover roughly 50 deg^2 divided over six fields separated on the sky (Lonsdale et al. 2003). We use a simple color selection to identify high–redshift galaxies from *Spitzer*/IRAC 3.6 and 4.5 μm photometry. As discussed in Papovich (2008), >90% of galaxies with $z > 1.3$ have $([3.6]-[4.5])_{\rm AB} > -0.1$ mag. Papovich (2008) identified candidate galaxy clusters at $z > 1.3$ by selecting overdensities of $\gtrsim 30$ objects satisfying this color criterion within radii of 1.′4 (corresponding to $r < 0.7$ Mpc at $z = 1.5$) from the SWIRE survey data. IRC 0218–A was identified in Papovich (2008) in the SWIRE XMM-LSS field, and has astrometric coordinates, $\alpha = 2^h18^m21.3^s$, $\delta = -05°10'27''$ (J2000), derived from the centroid of the IRAC sources in this overdensity. The left panel of figure 1 shows a false–color image using the *B*–band (blue), i'–band (green) and 4.5 μm image (red) of the field centered on the coordinates of the IRAC–selected overdensity.

[12] Throughout we denote magnitudes measured in the 3.6, 4.5, 5.8, and 7.9 μm IRAC channels as [3.6], [4.5], [5.8], and [8.0], respectively.

2.2. *Optical and Near–IR Imaging*

The XMM-LSS includes deep optical (0.4–1 μm) and near–IR imaging (1–2 μm) in a portion of the field covering roughly 0.70 deg^2. Optical imaging is available from the Subaru–XMM Deep Survey (SXDS, Furusawa et al. 2008), which provides imaging from the Subaru Prime Focus Camera (Suprime–Cam) in the broad bandpasses *B*, *R*, i', and z'. Near–IR imaging is available from the UKIRT Infrared Deep Sky Survey (UKIDSS, data release 1, Lawrence et al. 2007) ultra deep survey (UDS) in the broad bandpasses *J* and *K*. For the work here, we utilize the *K*–selected catalog of the SXDS and UDS data from Williams et al. (2009). These catalogs reach 5σ–limiting magnitudes in 1.″75–diameter apertures of $B_{\rm AB} < 27.7$, $R_{\rm AB} < 27.1$, $i_{\rm AB} < 26.8$, $z_{\rm AB} < 25.5$, $J_{\rm AB} < 24.9$, and $K_{\rm AB} < 23.6$ mag. The *K*–selected catalogs also include quasi–total *K* magnitudes, measured in elliptical apertures based on the light profile for each source. For details, we refer the reader to Williams et al. (2009). We scaled the aperture magnitudes measured in each band by the difference between the aperture and total *K*–band magnitudes, $K({\rm ap}) - K({\rm tot})$, to produce total (aperture corrected) magnitudes in each band.

2.3. *Spitzer IRAC Imaging*

We combine the SXDS optical and UDS near–IR catalog with deeper IRAC and MIPS imaging data from the *Spitzer* public legacy survey of the UKIDSS UDS (SpUDS, PI: J. Dunlop). These data are substantially deeper than those available with the SWIRE survey data. We measured photometry in 4″–diameter apertures in each of the IRAC 3.6, 4.5, 5.8, and 8.0 μm images. We applied correction factors of 0.32, 0.36, 0.55, 0.68 mag, respectively, which corrects these aperture magnitudes to total magnitudes for point sources. We matched the sources in each of the IRAC–selected catalogs to those in the *K*–selected catalog within 1″ radii. We combined the "total" aperture–corrected magnitudes for the IRAC data with the aperture corrected photometry for the SXDS and UDS data.

2.4. *Photometric Redshifts and the Integrated Redshift Probability*

The merged SXDS, UDS, and IRAC catalog covers a wavelength baseline of 0.4–8 μm, and we used these data to study the cluster–candidates selected from the SWIRE IRAC data. We derived photometric redshifts for each source in the *K*–selected catalog using EAZY (Brammer et al. 2008). We used the default galaxy spectral energy distribution templates with a *K*–band prior based on the luminosity functions of galaxies in a semi–analytic simulation. We derive the most likely photometric redshift as well as the full photometric–redshift probability distribution function, $P(z)$, normalized such that $\int P(z)dz = 1$ when integrated over all redshifts. Our comparisons against the spectroscopic redshifts in the SpUDS field (Yamada et al. 2005; Simpson et al. 2006; van Breukelen et al. 2007, 2009, and Akiyama et al. in preparation) show that the most likely photometric redshifts have a standard deviation (from the normalized median absolute deviation Beers et al. 1990) of $\Delta([z_{\rm sp} - z_{\rm ph}]/[1 + z_{\rm sp}]) = 0.04$ for

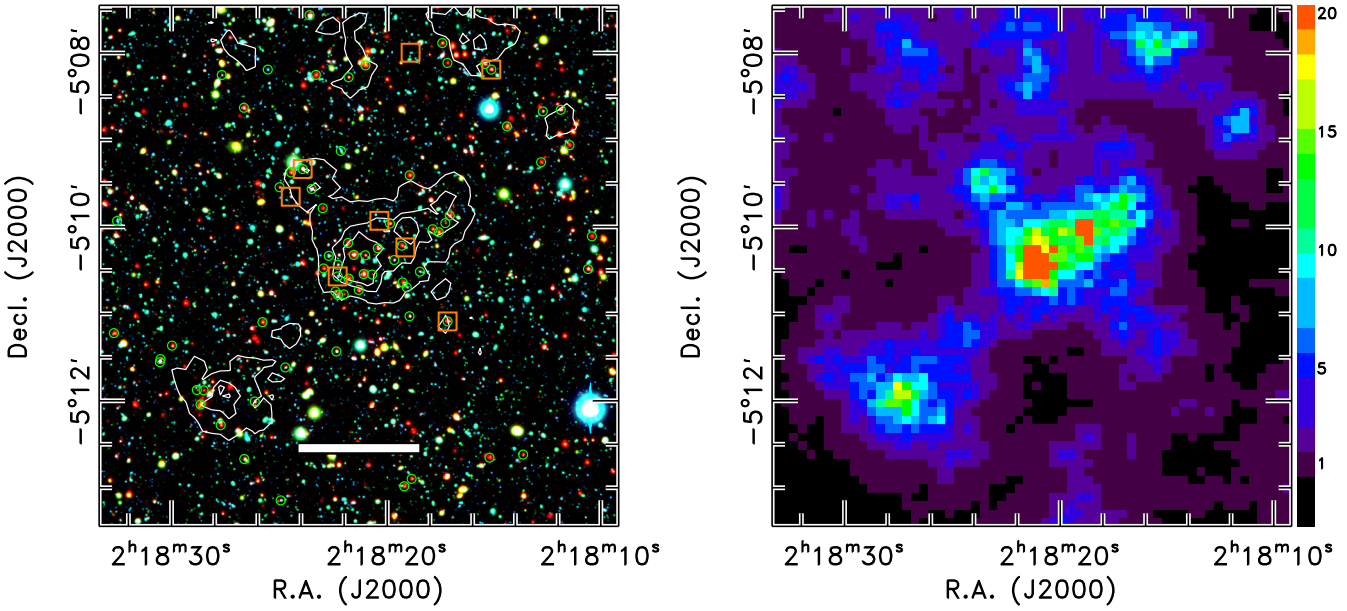

Figure 1. The left panel shows a false–color image of the target field. Blue corresponds to the Suprime *B*–band, Green to the Suprime *i*–band, and Red to the *Spitzer* 4.5 μm band. The images have not been corrected for variations in the data image quality. The image spans $6' \times 6'$, corresponding to 3 Mpc $\times$ 3 Mpc at $z = 1.62$. The heavy white bar shows a distance of 0.7 Mpc at the redshift of the cluster. Small green circles denote candidate cluster members with $\mathcal{P}_z > 0.5$ as defined in § 2.4. Orange squares denote those objects with spectroscopically confirmed redshifts $1.62 < z < 1.65$. The contours denote regions with 5, 10, and 15σ above the mean density of galaxies with $1.5 < z_{\rm phot} < 1.7$. The right panel shows the surface density of galaxies with $1.5 < z_{\rm phot} < 1.7$ in units of the number of standard deviations (σ) above the mean density, ranging from -1 to 20 (as indicated in the plot legend).

the more than 200 galaxies (excluding broad–line AGN) with spectroscopic redshifts in the range $1.0 \leq z \leq 2.0$.

To identify the highest priority galaxy overdensities for spectroscopic observations, we used our photometric redshifts in the UDS field to measure the surface density of galaxies in coarse redshift intervals. We then correlated this with the IRAC–selected sample using the SWIRE data covering the much larger area to identify probable high–redshift galaxy overdensities. To measure the surface density of galaxies, we divided galaxies into redshift intervals, $\Delta z = 0.2$, and measured the angular distance from each object to the seventh–nearest neighbor, d_7, and then computed the corresponding surface density, $\Sigma_7 \propto (d_7)^{-2}$. We tested other definitions for the nearest neighbor, which produced similar results (changing the definition of the *N*th–nearest neighbor changed primarily the angular resolution of the surface density map). We then calculated the mean and standard deviation of the surface density across the entire UDS field.

IRC 0218–A appears as a strong overdensity of galaxies with $1.5 < z_{\rm ph} < 1.7$. Figure 1 (right panel) shows the surface density of galaxies in this photometric–redshift range centered on the IRAC–selected overdensity IRC 0218–A. The color shading corresponds to the number of standard deviations above the mean surface density of galaxies at this redshift over the UDS field. IRC 0218–A corresponds to a $> 20\sigma$ surface density of galaxies in this redshift interval.

Many of the galaxies in the field of IRC 0218–A have photometric redshifts centered tightly around $z_{\rm ph} \simeq 1.6$. We quantified the likelihood of galaxies being associated in redshift by defining the *integrated redshift probability*,

$$\mathcal{P}_z \equiv \int P(z)\,dz, \qquad (1)$$

integrated over $z = z_{\rm cen} \pm \delta z$. For IRC 0218–A, we used $z_{\rm cen} = 1.625$ and $\delta z = 0.05 \times (1 + z_{\rm cen})$ (therefore integrating over $1.49 < z < 1.76$), approximately the 68% confidence range on the photometric redshifts. This is motivated by other cluster–member selection methods using photometric–redshift–selected samples (Brunner & Lubin 2000; Halliday et al. 2004; Eisenhardt et al. 2008; Pelló et al. 2009). Simply defined, the integrated redshift probability is the fraction of the photometric redshift probability distribution function within the redshift intervals (see discussion in Finkelstein et al. 2009). An integrated probability of $\mathcal{P}_z = 0.5$ means that 50% of the integrated photometric redshift distribution lies between $z_{\rm cen} - \delta z < z < z_{\rm cen} + \delta z$. The galaxies in the field of IRC 0218–A with $\mathcal{P}_z > 0.5$ are indicated in figure 1.

2.5. *Spectroscopic Observations*

We targeted galaxies with high integrated redshift probability in the region of IRC 0218–A using the *Inamori Magellan Areal Camera and Spectrograph* (IMACS) on the Magellan/Baade 6.5 m telescope on 2008 Oct 30–31, 2008 Nov 18–19, and again on 2009 Sep 11–12. At the f/2 focus IMACS provides multiobject spectroscopic observations over a 27.2′–diameter field of view (FOV), which allows us to target roughly 100 cluster–candidate galaxies using a single slitmask. We targeted two separate IMACS fields within the UDS, covering 10 cluster candidates in field 1 and 6 in field 2, using two slitmasks per field to alleviate slit collisions. IRC 0218–A was one of our highest priority targets given the high surface density of objects with high $\mathcal{P}_z$. The other cluster candidates will be discussed in a forthcoming paper.

We observed with IMACS using the 200 lines/mm grating with the OG570 blocking filter, which provided $\sim$7 Å resolution covering $0.6 - 1$ μm. The IMACS CCDs were upgraded in 2008 and have very high red sensitivity, with about a factor of two improvement in sensitivity beyond 8500 Å (A. Dressler 2008, private communication). We observed using the "nod–and–shuffle" mode (Glazebrook & Bland-Hawthorn

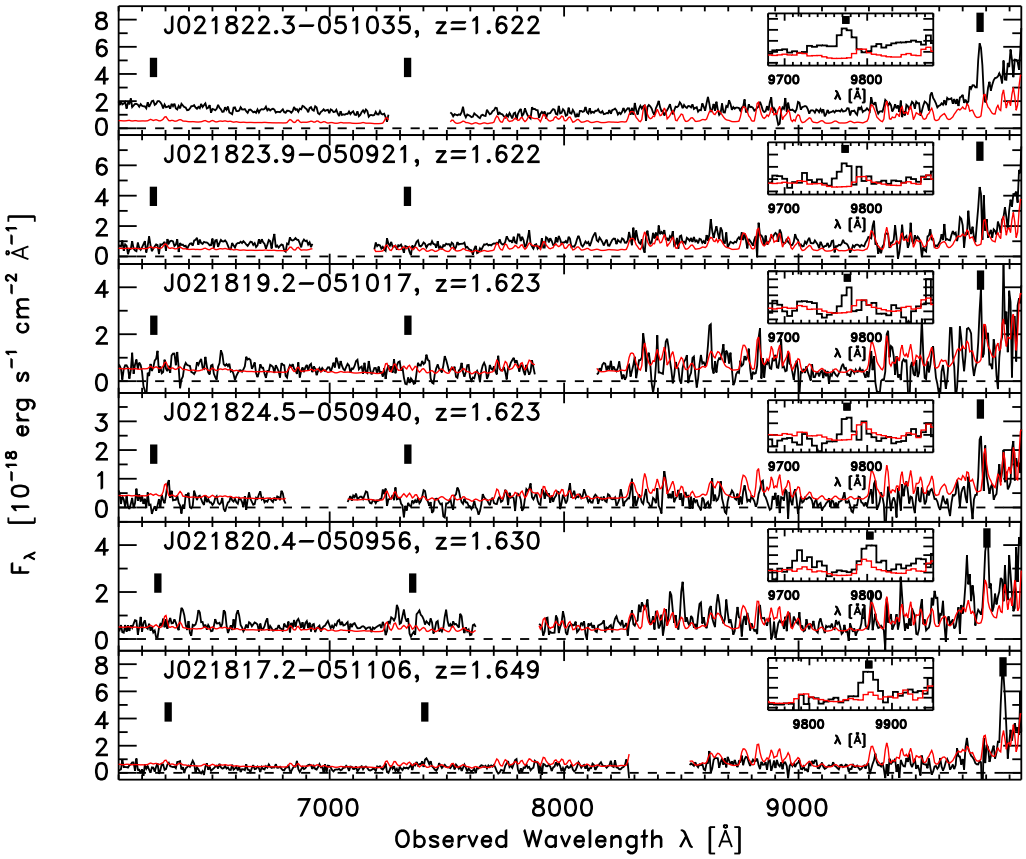

Figure 2. Extracted IMACS spectra for the six galaxies with $1.62 < z < 1.65$ within $1.4'$ from the cluster center (corresponding to $r < 0.7$ Mpc at $z = 1.62$). The inset panel shows the region around [O II] λ3727 at the measured redshift. In all panels, the black line is the measured spectrum. Gaps in the spectra show wavelengths that fall on the "gaps" between the IMACS CCDs. The red line shows the 1σ uncertainties propagated through the data reduction. The thick black lines show the locations of Fe II λ2374, Mg II λ2800, and [O II] λ3727 for the measured redshift.

Table 1
Spectroscopic Redshifts in the IRC 0218–A Field

Identifier	$\mathcal{P}_z$	z	σ_z	R (mag)	Δ ($'$)	r (Mpc)
(1)	(2)	(3)	(4)	(5)	(6)	(7)
J021822.3–051035	0.50	1.6224	0.0005	23.1	0.28	0.14
J021820.4–050956	0.42	1.6303	0.0012	23.8	0.57	0.29
J021819.2–051015	0.47	1.6230	0.0005	23.2	0.57	0.29
J021824.1–050945	0.46	1.5356	0.0004	23.4	0.99	0.51
J021824.5–050940	0.40	1.6228	0.0005	23.6	1.12	0.57
J021817.2–051106	0.61	1.6487	0.0006	24.0	1.21	0.61
J021823.9–050921	0.54	1.6222	0.0005	23.0	1.29	0.65
J021818.9–050800	0.32	1.6234	0.0013	23.9	2.52	1.28
J021815.2–050812	0.64	1.6224	0.0011	24.0	2.72	1.38
J021814.5–050659	0.47	1.6094	0.0008	23.7	3.86	1.96

Note. — (1) Galaxy Identifier from J2000 coordinates, (2) Integrated redshift probability, (3) spectroscopic redshift, (4) redshift uncertainty, (5) Suprime R–band magnitude, (6) angular separation between the galaxy and the cluster astrometric center, (7) physical separation between galaxy and the cluster center for $z = 1.62$.

2001) with $1'' \times 2.2''$ slitlets, which greatly improves the background subtraction and facilitated our spectroscopic redshift success, especially for galaxies at $z > 1.3$. For practical purposes, we prioritized galaxies with $R < 23.5$ mag, but included galaxies to $R < 23.9$ mag (and a few even fainter galaxies). The total effective exposure times for each mask were approximately 6 hours on source.

We reduced the IMACS spectroscopic data using the Carnegie Observatories System for MultiObject Spectroscopy (COSMOS, v2.13)[13]. The reduction steps to produce 2D spectra include wavelength calibration, bias subtraction, flat fielding, sky subtraction, co–adding the separate frames, and cosmic–ray removal. We extracted 1D spectra at each nod–and–shuffle position separately, as well as the associated uncertainty on the spectra propagated through the reduction pipeline. We then coadded the individually extracted 1D spectra for each target. We used spectrophotometric standards taken at the end of each night to provide flux calibration.

We measured spectroscopic redshifts for 10 galaxies with an angular separation of $\Delta < 4'$ of the astrometric center of IRC 0218–A (corresponding to a physical separation of $r < 2.0$ Mpc at $z = 1.62$). These are presented in table 1. In all cases, the redshifts are secured on the basis of the [O II] emission line. We inspected the 2D reduced data and verified that the emission feature is present in both *independent* spectra obtained from the nod–and–shuffle observation. All of these galaxies were targeted as candidate members of this galaxy cluster. Seven of the galaxies have $1.62 < z < 1.63$ with a mean $\langle z \rangle = 1.622$. Of the remaining galaxies, two have $z = 1.649$ and 1.609 (velocity separations <3000 km s^{-1}), and the other has $z = 1.536$. If we include all nine galaxies within 3000 km s^{-1}, then we derive a mean redshift $\langle z \rangle = 1.625$.

Figure 2 shows the one–dimensional spectra for six galaxies with $1.62 < z < 1.65$ with the smallest angular separation ($\Delta < 1.'4$) from the astrometric center of IRC 0218–

[13] http://obs.carnegiescience.edu/Code/cosmos

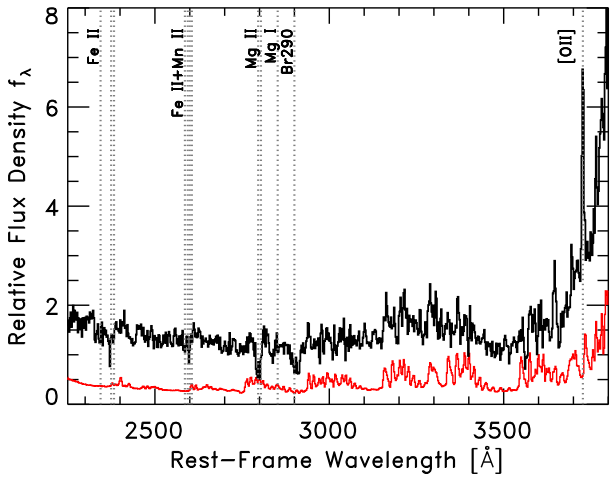

Figure 3. Composite one–dimensional IMACS spectra as a function of rest–frame wavelength for the seven galaxies within $r < 1.4$ Mpc of the astrometric center of IRC 0218–A with spectroscopic redshifts $1.620 \leq z \leq 1.630$ (see Table 1). The black line shows the composite, weight–averaged spectrum, and the red line is the weighted uncertainty, dominated by emission from the sky. Strong [O II] is observed, as well as several absorption features, including the doublet Mg II$\lambda\lambda$2976,2804, and absorption from blends of Fe II line. There is an unidentified feature at 2900 Å, possiblly associated with the spectral break noted by Spinrad et al. (1997).

A. Each spectrum shows the presence of [O II] in emission. Several of the spectra show evidence for interstellar absorption from Mg II and possibly Fe II (one galaxy at $z = 1.649$ shows weak Mg II emission, likely from an AGN). As the rest of the absorption features are weak, we show in figure 3 a weighted–mean, composite spectrum for the seven galaxies with $1.62 < z < 1.63$, all within $r < 1.4$ Mpc. To construct this spectrum, we scaled each spectrum to the mean flux density in the rest–frame wavelength range 2600–3100 Å. We then weighted each spectrum by the inverse variance using the uncertainty spectrum. Strong emission from [O II] λ3727 is observed in the composite spectrum, which is a result of the spectroscopic identification process. The stacked spectrum shows several strong absorption features, in particular Mg II $\lambda\lambda$2976,2804, Mg I λ2851 and absorption from various blends of Fe II lines.

The narrow redshift range of the galaxies in table 1 suggests they are physically associated. Using the spectroscopic redshifts to infer the dynamical conditions of the cluster is dubious because of the unknown dynamical state (see § 4.2). If we assume the galaxies within $<$1500 km s^{-1} of the mean redshift and within 0.9 Mpc of the astrometric center of the IRAC–selected overdensity sample adequately a virialized structure, then their redshifts correspond to a line–of–sight velocity dispersion of $\sigma = 860 \pm 490$ km s^{-1} using the definition in Carlberg et al. (1996). The uncertainty is derived from a bootstrap resampling of the data (and we make no attempt to remove the additional uncertainty from the redshift errors). However, we further qualify this velocity dispersion because of several biases that likely affect the redshift success rate for galaxies in this cluster. Firstly, we prioritized only those galaxies with $R < 23.9$ mag for spectroscopy, preferentially excluding fainter galaxies. Second, even with this magnitude criterion, most of the galaxies are faint ($23 < R < 24$ mag) and all the redshift identifications above are based primarily on the [O II] λ3727 emission line. At $z = 1.62 - 1.63$, this line falls at 9780 – 9800 Å, adjacent to a strong sky line at 9800 Å, which hinders the identification of galaxies at $z \approx 1.63$ with emission lines (the only galaxy at this redshift identified above includes strong Mg II absorption). Therefore, our spectroscopic redshifts will be biased against objects at $z \approx 1.63$. If the cluster lies at $z = 1.625$ then roughly half the galaxies with redshifts in the upper end of the distribution will be preferentially missed, biasing the mean redshift and the velocity dispersion measurement. Therefore, while we conclude the galaxies are physically associated as a galaxy (proto–)cluster, we caution against too much interpretation of the dynamics of this cluster using the redshifts above.

3. THE NATURE OF IRC 0218–A

In this section we discuss the evidence that IRC 0218–A is a galaxy (proto–)cluster. Strictly speaking, a "cluster" is an object that is fully virialized, while a "proto–cluster" is an object that will eventually virialize at later times (lower redshift). It remains to be seen if the dark–matter halo of IRC 0218–A is fully virialized or if it is still assembling. Nevertheless, we will blur the distinction between these definitions and use the term "cluster" to mean both.

The photometric redshift distributions and spectroscopic redshifts of galaxies in IRC 0218–A indicate a large overdensity of galaxies at $z = 1.62$ with a high surface density within $r < 0.7$ Mpc. This is illustrated in figure 1. The galaxies with spectroscopic redshifts in this region of high surface density show a preponderance of redshifts around $z = 1.62$. Furthermore, the IRAC–selected galaxy members of this cluster have high integrated redshift probability as defined in equation 1, implying a high likelihood of being at the cluster redshift. Galaxies with $\mathcal{P}_z > 0.5$ are indicated with circles in figure 1. This includes many red galaxies, which are concentrated near the center of IRC 0218–A and have very high $\mathcal{P}_z$ values.

Figure 4 shows a montage of photometric redshift probability distribution functions, $P(z)$, for the seven galaxies with the highest integrated redshift probabilities, $\mathcal{P}_z$, with an angular separation of $\Delta < 1'$ of the cluster center. Without exception these galaxies have red $(z-J)$ colors. We targeted several of these galaxies with spectroscopy from IMACS during our 2009 observing run. However, their spectra show only faint optical continua, with no discernible emission features. Nevertheless, while we are unable to derive spectroscopic redshifts for these galaxies, the lack of any emission features is consistent with their photometric redshifts. The photometric redshifts of these galaxies are driven by the strength of the apparent 4000 Å/Balmer break redshifted between the z- and J-bands at $z = 1.62$. As a result, the photometric redshift $P(z)$ functions are sharply peaked at this redshift, and these galaxies have $\mathcal{P}_z > 0.75$, implying that more than 75% of their redshift probability lies between $1.49 < z < 1.76$ with a most likely redshift at $z \simeq 1.62$, the mean spectroscopic redshift.

In contrast, the galaxies for which we obtained spectroscopic redshifts have lower $\mathcal{P}_z$. These galaxies all show [O II] in their spectra, implying relatively recent star formation, implying they have weaker 4000 Å/Balmer breaks and subsequently less-well constrained $P(z)$. This is illustrated in figure 4, which shows the $P(z)$ for the seven galaxies with spectroscopic redshifts at that of the cluster. All of these galaxies have bluer $(z-J)$ colors, consistent with the evidence of more recent star formation.

The red galaxies in this overdensity dominate the color–magnitude relation for this cluster, similar to the relations observed in clusters at $z \lesssim 1$ (e.g., Bower et al. 1992; Ellis et al.

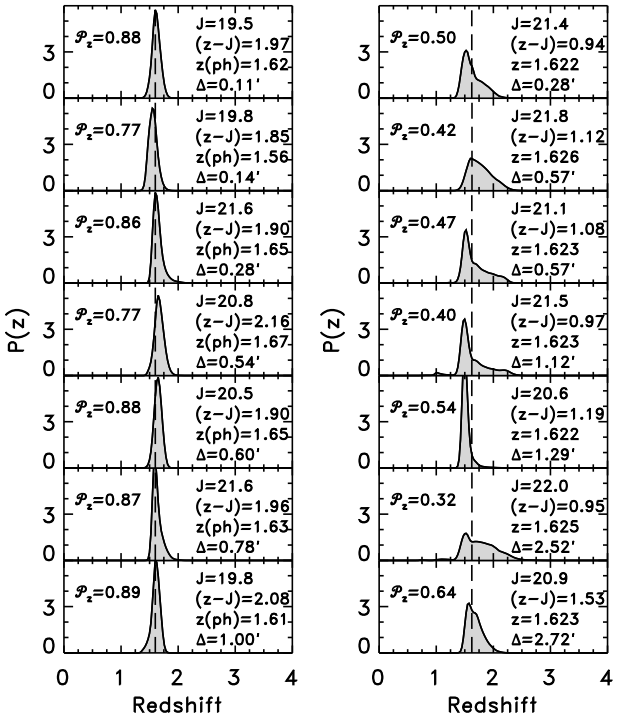

Figure 4. Photometric–redshift probability–distribution functions, $P(z)$, for galaxies in IRC 0218–A. The left figure shows the $P(z)$ for the seven galaxies that have integrated redshift probabilities, $\mathcal{P}_z > 0.75$ with angular separations of $\Delta < 1'$ of the cluster center. Without exception, these galaxies all have very red $(z-J)$ colors. Each panel gives the $(z-J)$ color, J-magnitude, the most likely photometric redshift, the integrated redshift probability, and angular separation from the cluster center. Although these galaxies lack spectroscopic information, their large integrated redshift probabilities support the assertion that they are at the cluster redshift, $z = 1.62$, indicated by the vertical dashed lines. The cluster galaxies with spectroscopic redshifts all show [O II] in their spectra, implying ongoing star formation (see figure 2). They have bluer $(z-J)$ colors and lower values of $\mathcal{P}_z$, presumably because they have weaker 4000 Å/Balmer breaks owing to the star formation activity. The right figure shows the $P(z)$ for the seven galaxies with spectroscopic redshifts $1.62 < z < 1.63$. Each panel shows the same information as for the left figure, except that they give the spectroscopic redshift instead of the most likely photometric redshift.

1997; Stanford et al. 1998; van Dokkum et al. 1998a,b; Blakeslee et al. 2006; De Lucia et al. 2007; Tran et al. 2007; Mei et al. 2009). Figure 5 shows a $z-J$ versus J color–magnitude diagram for *all* galaxies within 2 arcmin ($r <$ 1 Mpc at $z = 1.62$) of the astrometric center of the IRAC–selected overdensity. The z and J bandpasses span the redshifted 4000 Å/Balmer break at redshift $z = 1.62$ providing strong contrast between the cluster galaxies and those in the field. Field galaxies are shown as small data points in figure 5, and these have $\mathcal{P}_z < 0.3$, implying they are foreground or background galaxies. Larger symbol sizes correspond to higher values of $\mathcal{P}_z$, implying those objects have a greater likelihood of being at the cluster redshift. The cluster galaxies on the red–sequence typically have the highest values of $\mathcal{P}_z$, especially at the bright end where photometric uncertainties have a smaller effect on the colors. The well–defined color–magnitude relation in IRC 0218–A is evidence for the cluster–like nature of this object. This is the highest redshift spectroscopically confirmed cluster with such a well–defined red sequence.

The red galaxies that dominate IRC 0218–A are centrally concentrated, and nearly all are within $\Delta < 1'$ of the cluster center. Very few of the galaxies on the red sequence have angular separations $>1'$. Of the few that have larger angular separations, most reside within the surface–density contours that extend slightly to the north–east and north–west from the central region (see figure 1). This property of IRC 0218–A is consistent with the color–density relations observed in lower–redshift clusters (e.g., Dressler 1980; Mei et al. 2009) providing further support for the cluster–like nature of IRC 0218–A.

In summary, the spectroscopic and photometric redshifts, the color–magnitude relations, and the surface density–color relations all support the conclusion that IRC 0218–A is a galaxy cluster. We therefore conclude these galaxies are physically associated with each other as a cluster, even though we do not have the data to determine if they are fully virialized. In the next section we discuss the properties of this object and the cluster galaxies.

4. DISCUSSION

From the evidence presented above, we conclude that IRC 0218–A represents a galaxy cluster at $z = 1.62$. Although other candidates for high–redshift galaxy (proto–)clusters at $z > 1.5$ have been reported (e.g., Miley et al. 2004; Brodwin et al. 2007; McCarthy et al. 2007; Zirm et al. 2008; Eisenhardt et al. 2008; Andreon et al. 2009; Kurk et al. 2009; Chiaberge et al. 2010), this is the highest redshift, spectroscopically–confirmed cluster with a strong, well–defined red sequence. While the definition of galaxy "cluster" may be subject to semantics (see above), IRC 0218–A shows all the characteristics indicative of lower–redshift, rich galaxy clusters.

The fact that IRC 0218–A has a well–defined red sequence of strongly clustered red galaxies is not a result of the selection method. IRC 0218–A was selected as an overdensity of galaxies with red IRAC colors (see § 2.1). The IRAC colors at this redshift are blind largely to variations of rest–frame optical colors, and should be sensitive to galaxies with both rest–frame red and blue UV–optical colors (see Papovich 2008). With our full sample, we will compare the properties of IRC 0218–A against other overdensities of galaxies at this redshift to determine how the galaxies in this object compare to other co–eval (proto–)clusters and to field galaxies.

4.1. *Color Evolution and Formation Epoch*

As discussed above, IRC 0218–A is dominated by a strong red sequence of bright galaxies. These are intrinsically very luminous for their redshift, $z = 1.62$. The top axis of figure 5 compares the measured J–band magnitudes to the "characteristic" magnitude, J^*, for the luminosity function of galaxies in the Coma cluster, evolved passively backwards in time to $z = 1.62$ using the model of de Propris et al. (1999). The brightest galaxies in IRC 0218–A correspond to $J^* - 1$ to $J^* - 1.5$ mag. The descendants of these galaxies at a minimum will be super–L^* cluster galaxies by $z \sim 0$, even without subsequent merging or star formation.

The red galaxy colors implies that they contain older stellar populations. Figure 5 illustrates the expected color of a composite stellar population formed at $z_f = 3$ with a star–formation rate that evolves by an e–folding timescale $\tau = 0.1$ Gyr to $z = 1.62$ using the 2007 version of the Bruzual & Charlot (2003) models. This model produces a $(z-J)$ color similar to what we measure for the brighter red galaxies in this cluster. There is also no indication that IRC 0218–A contains a population of blue, luminous galaxies. The brightest galaxies within a projected separation

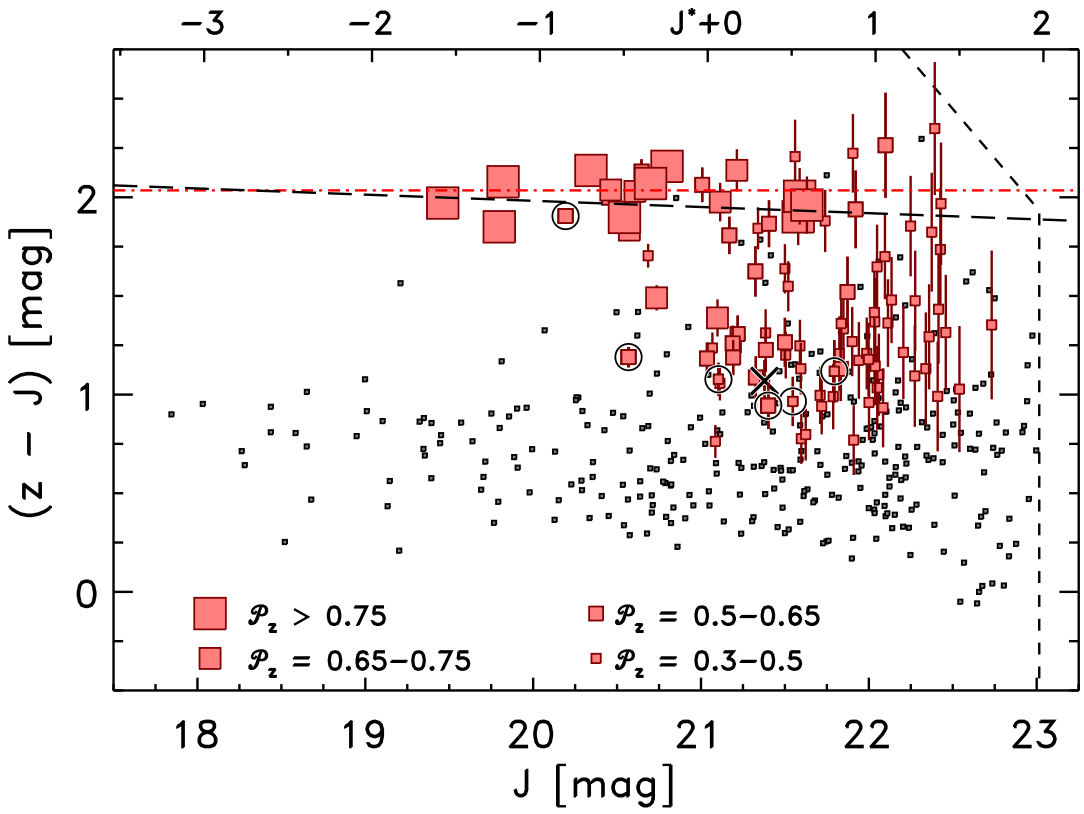

Figure 5. Color–magnitude diagram of all galaxies within $\Delta < 2'$ of the cluster center, corresponding to 1 Mpc at $z = 1.62$. The top axis shows magnitudes in units of J^*, the characteristic luminosity evolved from the measured values for the Coma cluster (de Propris et al. 1999) to $z = 1.62$. The symbol size denotes that likelihood that the galaxy lies at the cluster redshift based on the integrated redshift probability, P_z, as indicated in the legend. The smallest gray squares all have $\mathcal{P}_z < 0.3$, and are likely foreground or background field galaxies, unassociated with the cluster. Larger, red squares correspond to galaxies with $\mathcal{P}_z > 0.3$, and likely associated with the cluster. The long–dashed line shows a fit to the red sequence (see § 4). The red dot-dashed line shows the expected color of a stellar population observed at $z = 1.62$ formed in a short burst at $z_f = 3$ as described in the text. Circles denote those objects spectroscopically confirmed from $1.62 < z < 1.65$. These are bluer galaxies owing to the presence of [O II] emission, facilitating their spectroscopic identification (see § 2.5). The X symbol shows an object with a spectroscopic redshift outside this range. The short dashed line indicates the magnitude limits for the imaging data. A strong red–sequence is apparent, which is dominated by galaxies with high $\mathcal{P}_z$.

of $r < 1$ Mpc of IRC 0218–A with $(z-J) < 1.5$ mag and $\mathcal{P}_z > 0.3$ have fainter magnitudes, typically sub–J^*. Because the mass–to–light ratios of the stellar populations increase as they redden and fade over time, the dominant population of red–sequence galaxies could not form directly from the less–luminous blue galaxies. Interestingly, the number of red sequence galaxies appears to decline toward the faint end of the red sequence, seemingly at magnitudes well above the detection limit (see figure 5). This may imply a strong evolution in the faint end of the red–sequence luminosity function, extending the relation measured by Rudnick et al. (2009) for moderate redshift clusters to higher redshift. It also appears that there is a lack of faint blue galaxies with $\mathcal{P}_z > 0.3$ but no such lack is seen in the $\mathcal{P}_z < 0.3$ galaxies, indicating that the photometry is indeed complete to the level indicated in the figure. Further studies of clusters at these redshifts and detailed modeling are needed to confirm this.

The zeropoint, scatter, and slope of the red sequence itself provide constraints on the formation timescales of the galaxies' stellar populations (e.g., Bower et al. 1992; Aragon-Salamanca et al. 1993). To compare the galaxies in IRC 0218–A at $z = 1.62$ to those in lower redshift clusters, we converted the observed $(z-J)$ colors to rest–frame $(U-B)_0$ colors[14] following Mei et al. (2009). We find no evidence for evolution in the slope of the red sequence between IRC 0218–A and lower redshift galaxy clusters, consistent with the results of other studies (see, e.g., Mei et al. 2009). The top panel of figure 6 shows the rest–frame $(U-B)_0$ color of IRC 0218–A and lower redshift clusters taken from the literature at a fixed absolute magnitude, $M_{B,0} = -21.4$ mag. However, there is strong evolution in the rest–frame $(U-B)_0$ colors, which become redder with decreasing redshift, consistent with passive evolution. The models in figure 6 illustrate the expected evolution for stellar populations with different formation redshifts ($z_F = 2.0$, 2.5, 3.0, and 5.0), with a star–formation e–folding timescale, $\tau = 0.1$ Gyr, and solar metallicity. The $(U-B)_0$ color at $M_B = -21.4$ mag for IRC 0218–A is consistent with stellar populations formed between $2.0 \lesssim z \lesssim 2.5$.

We model the scatter in the colors of the red–sequence galaxies in IRC 0218–A by following Hilton et al. (2009, and references therein). We construct a series of composite stellar populations with star–formation e–folding timescale of $\tau = 0.1$ Gyr and solar metallicity. We tested other values for the metallicity (ranging from 0.2 $Z_\odot$ and 2.5 $Z_\odot$), but found that they did not reproduce simultaneously the zeropoint and scatter in the $(U-B)_0$ colors for a consistent formation epoch. In these models, a galaxy begins to form stars at an initial formation redshift, z_F, for a period Δt, where Δt varies from $\Delta t = 0$ to the epoch at which the cluster is observed. For each z_F, we construct a simulated sample of 10^5 galaxies

[14] We use the subscript 0 on $(U-B)_0$ to denote the $z = 0$ rest-frame color.

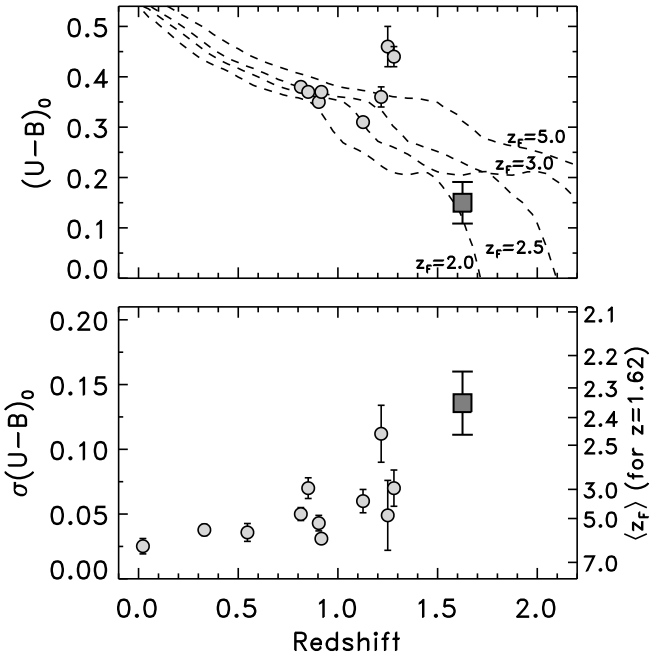

Figure 6. The top panel shows the evolution of the rest–frame $U-B$ color measured at $M_{B,0} = -21.4$ mag for red–sequence galaxies in clusters as a function of redshift. Smaller circles show the results from lower–redshift clusters (Bower et al. 1992; Ellis et al. 1997; van Dokkum et al. 1998a,b, 2000; Mei et al. 2009). The large box point shows the value derived for the cluster IRC 0218–A at 1.625 derived here. The curves show the expected evolution of a stellar population with solar metallicity formed with an e–folding timescale $\tau = 0.1$ Gyr at the formation redshift indicated. The bottom panel shows the evolution of the scatter in the rest–frame $U-B$ color for red–sequence galaxies as a function of redshift. Symbols are the same as the top panel. The scatter in the colors of red–sequence galaxies increases with redshift. The right axis of the bottom panel indicates the expected scatter in the $(U-B)_0$ color for a red sequence observed at $z = 1.62$ for a given mean luminosity–weighted formation redshift (see text). The scatter in the $(U-B)_0$ color for the $z = 1.62$ cluster corresponds to a luminosity–weighted formation redshift of $\bar{z_f} = 2.25-2.45$, consistent with the evolution in the $(U-B)_0$ color.

with ages assigned randomly from a uniform distribution with $0 < t < \Delta t$, and we compute the scatter in the simulated color distributions as a function of the luminosity–weighted age. We use the value of the luminosity–weighted age for a measured color scatter to infer the formation redshift.

We calculated the scatter for the red sequence galaxies in IRC 0218–A, using the scatter about the median absolute deviation (Beers et al. 1990), which gives a scatter of $\sigma(U-B)_0 = 0.136 \pm 0.024$. We compare this to the red sequences of other galaxy clusters and our models in the bottomw panel of figure 6. There is a marked increase in the scatter in the $(U-B)_0$ color with redshift, as expected as cluster galaxies are observed closer in time to when they formed their stellar populations (e.g., Mei et al. 2009; Hilton et al. 2009). The right axis of the panel indicates the modeled relationship between $\sigma(U-B)_0$ and the formation redshift, z_f for the model stellar populations observed at $z = 1.62$. The scatter in $(U-B)_0$ color for IRC 0218–A corresponds to range of formation redshift, $2.25 \leq z \leq 2.45$. We note that this is an upper limit as we have made no attempt to remove the color measurement uncertainties from the intrinsic scatter. If we have overestimated the scatter, the formation redshift will be *higher*. Given the agreement between the formation epochs derived from the red-sequence zeropoint and scatter, we do not think this is a serious effect.

Therefore, both the zeropoint and scatter of the rest–frame $(U-B)_0$ colors for red–sequence galaxies in IRC 0218–A imply a formation epoch of $z_f \simeq 2.25-2.45$ (a lookback time of $1.0-1.3$ Gyr from $z = 1.62$). This corresponds to the last major star–formation episode in these red cluster galaxies during which most of their stellar mass formed. This is a similar formation epoch as found in studies of other $z > 1$ cluster galaxies (e.g., Mei et al. 2009; Hilton et al. 2009), and consistent with the colors and spectral indices of galaxies in lower–redshift massive clusters (e.g., Stanford et al. 1998; van Dokkum & van der Marel 2007). Furthermore, studies show that a high fraction of massive galaxies at $z > 2$ have high levels of star formation (e.g., Kriek et al. 2006; Papovich et al. 2006), and these are likely consistent with the evolution of the cluster galaxies. These properties all support the conclusion that the galaxies of IRC 0218–A will become typical galaxies found in rich clusters at later times.

4.2. *Dynamical Mass Estimate*

As discussed above, it is unclear if the cluster galaxies of IRC 0218–A sample a virialized, relaxed dark–matter halo, or if this object is in the process of assembling through mergers. Under the assumption that the galaxies are virialized, we use the velocity dispersion to provide a crude estimate for the dynamical mass of IRC 0218–A as a reference, although we qualify this with the caveats in § 2.5. For a velocity dispersion, $\sigma = 860 \pm 490$ km s^{-1} (see § 2.5), the corresponding dynamical mass estimate is $M_{\rm dyn} \sim 3 r_{\rm vir} \sigma^2 \sim 4 \times 10^{14}\ M_\odot$ for a virial radius of 0.9 Mpc. We derive the same dynamical mass estimate using M_{200} (Carlberg et al. 1997).[15] Even so, we caution the reader that the dynamical mass may be highly uncertain given the statistical errors and systematic biases.

This mass is a factor of $\sim$4 larger than the limiting halo mass of the IRAC–selected clusters (Papovich 2008), and if accurate, then it implies IRC 0218–A resides in one of the most overdense environments in the SWIRE survey. In this case, based on the expected growth of dark–matter haloes (Springel et al. 2005) the mass of IRC 0218–A should increase to at least $10^{15}\ M_\odot$ by $z = 0.2$, becoming a rich cluster of galaxies comparable to the Coma cluster.

5. SUMMARY

We report the discovery of a spectroscopically confirmed galaxy cluster at z=1.62 located in the SWIRE XMM-LSS field. This cluster candidate was selected solely as an overdensity of sources with red *Spitzer*/IRAC colors, satisfying $([3.6]-[4.5])_{\rm AB} > -0.1$ mag, with no other selection criteria imposed. Photometric redshifts derived from SXDS (*BViz*-bands), UKIDSS-UDS (*JK*-bands), and SpUDS (3.6-8.0 micron) for the galaxies in and around this cluster show that this structure corresponds to a galaxy surface density of sources at $z = 1.6$ that is $> 20\sigma$ times the mean surface density at this redshift. This confirms that our selection of overdensities of sources with red IRAC colors identifies galaxy clusters at $z \geq 1.3$.

We obtained spectroscopic observations of galaxies in the cluster region using IMACS on the Magellan telescope. We measured redshifts for five galaxies in the range z=1.62–1.63,

[15] Here M_{200} is the mass of the dark matter halo within a spherical volume defined by radius r_{200} where the average density is 200 times the critical density at the observed redshift.

all within 1.4 arcmin (< 0.7 Mpc) of the cluster center. In addition, we measured spectroscopic redshifts for two sources with z=1.62-1.63 within $1.4-2.8$ arcmin ($0.7-1.4$ Mpc). The cluster appears to be dominated by red galaxies, with $(z-J) > 1.7$ mag. The photometric redshift distributions for the brightest red galaxies are centrally peaked at $z = 1.62$, coincident with the spectroscopically confirmed galaxies.

The $z-J$ versus J color–magnitude diagram of the galaxies in this cluster shows a strong red-sequence, which includes the dominant population of red galaxies. The rest–frame $(U-B)_0$ color and scatter of galaxies on the red-sequence are consistent with a mean luminosity–weighted age of $1.0-1.3$ Gyr, corresponding to a formation redshift $\overline{z_f} = 2.40 \pm 0.15$, and implying that most of the stellar mass in this cluster formed at that epoch.

We provide a crude estimate of the dynamical mass of IRC 0218–A, although this result is highly uncertain due to systematics in the data and owing to the unknown dynamical state of IRC 0218–A. Under the assumption that the dark matter halo of IRC 0218–A is virialized and relaxed, we estimate a dynamical mass based on the measured velocity dispersion, $M_{\rm dyn} \sim 4 \times 10^{14}\ M_\odot$ within a virial radius of $r_{\rm vir} \sim 0.9$ Mpc. If this is accurate, then we expect IRC 0218–A to evolve to a rich cluster with $M \sim 10^{15}\ M_\odot$ at $z = 0.2$ similar to the Coma cluster. Further spectroscopic and multiwavelength observations of galaxies in IRC 0218–A are needed to constrain better the mass measurement.

We acknowledge our colleagues for stimulating discussions, and helpful comments. In particular, we wish to thank Adam Stanford and Jon Willis. This work is based on observations made with the *Spitzer Space Telescope*, which is operated by the Jet Propulsion Laboratory, California Institute of Technology. This work is based in part on data obtained as part of the UKIRT Infrared Deep Sky Survey. A portion of the Magellan telescope time was granted by NOAO, through the Telescope System Instrumentation Program (TSIP). TSIP is funded by NSF. Support for M.B. was provided by the W. M. Keck Foundation. We acknowledge generous support from the Texas A&M University and the George P. and Cynthia Woods Institute for Fundamental Physics and Astronomy.

REFERENCES

Andreon, S., Maughan, B., Trinchieri, G., & Kurk, J. 2009, A&A, 507, 147
Aragon-Salamanca, A., Ellis, R. S., Couch, W. J., & Carter, D. 1993, MNRAS, 262, 764
Bahcall, N. A., Ostriker, J. P., Perlmutter, S., & Steinhardt, P. J. 1999, Science, 284, 1481
Beers, T. C., Flynn, K., & Gebhardt, K. 1990, AJ, 100, 32
Blakeslee, J. P., et al. 2006, ApJ, 644, 30
Borgani, S., et al. 2001, ApJ, 561, 13
Bower, R. G., Lucey, J. R., & Ellis, R. S. 1992, MNRAS, 254, 601
Brammer, G. B., van Dokkum, P. G., & Coppi, P. 2008, ApJ, 686, 1503
Brodwin, M., Gonzalez, A. H., Moustakas, L. A., Eisenhardt, P. R., Stanford, S. A., Stern, D., & Brown, M. J. I. 2007, ApJ, 671, L93
Brodwin, M., et al. 2006, ApJ, 651, 791
Brunner, R. J., & Lubin, L. M. 2000, AJ, 120, 2851
Bruzual, G., & Charlot, S. 2003, MNRAS, 344, 1000
Carlberg, R. G., Yee, H. K. C., Ellingson, E., Abraham, R., Gravel, P., Morris, S., & Pritchet, C. J. 1996, ApJ, 462, 32
Carlberg, R. G., et al. 1997, ApJ, 485, L13
Chiaberge, M., Capetti, A., Macchetto, F. D., Rosati, P., Tozzi, P., & Tremblay, G. R. 2010, ArXiv e-prints
De Lucia, G., & Blaizot, J. 2007, MNRAS, 375, 2
De Lucia, G., et al. 2007, MNRAS, 374, 809
de Propris, R., Stanford, S. A., Eisenhardt, P. R., Dickinson, M., & Elston, R. 1999, AJ, 118, 719
Dressler, A. 1980, ApJ, 236, 351
Eisenhardt, P. R. M., et al. 2008, ApJ, 684, 905
Eke, V. R., Cole, S., Frenk, C. S., & Patrick Henry, J. 1998, MNRAS, 298, 1145
Ellis, R. S., Smail, I., Dressler, A., Couch, W. J., Oemler, Jr., A., Butcher, H., & Sharples, R. M. 1997, ApJ, 483, 582
Finkelstein, S. L., Papovich, C., Giavalisco, M., Reddy, N. A., Ferguson, H. C., Koekemoer, A. M., & Dickinson, M. 2009, ApJ, submitted, arXiv:0912.1338
Furusawa, H., et al. 2008, ApJS, 176, 1
Gladders, M. D., & Yee, H. K. C. 2005, ApJS, 157, 1
Gladders, M. D., Yee, H. K. C., Majumdar, S., Barrientos, L. F., Hoekstra, H., Hall, P. B., & Infante, L. 2007, ApJ, 655, 128
Glazebrook, K., & Bland-Hawthorn, J. 2001, PASP, 113, 197
Haiman, Z., Mohr, J. J., & Holder, G. P. 2001, ApJ, 553, 545
Halliday, C., et al. 2004, A&A, 427, 397
Hilton, M., et al. 2009, ApJ, 697, 436
Hopkins, A. M., & Beacom, J. F. 2006, ApJ, 651, 142
Johnson, H. L. 1966, ARA&A, 4, 193
Kajisawa, M., Kodama, T., Tanaka, I., Yamada, T., & Bower, R. 2006, MNRAS, 371, 577
Kodama, T., Tanaka, I., Kajisawa, M., Kurk, J., Venemans, B., De Breuck, C., Vernet, J., & Lidman, C. 2007, MNRAS, 377, 1717
Kriek, M., et al. 2006, ApJ, 649, L71
Kurk, J., et al. 2009, A&A, 504, 331
Kurk, J. D., et al. 2000, A&A, 358, L1
Lawrence, A., et al. 2007, MNRAS, 379, 1599
Lonsdale, C. J., et al. 2003, PASP, 115, 897
McCarthy, P. J., et al. 2007, ApJ, 664, L17
Mei, S., et al. 2009, ApJ, 690, 42
Miley, G. K., et al. 2004, Nature, 427, 47
Mullis, C. R., Rosati, P., Lamer, G., Böhringer, H., Schwope, A., Schuecker, P., & Fassbender, R. 2005, ApJ, 623, L85
Muzzin, A., et al. 2009, ApJ, 698, 1934
Oke, J. B., & Gunn, J. E. 1983, ApJ, 266, 713
Papovich, C. 2008, ApJ, 676, 206
Papovich, C., et al. 2006, ApJ, 640, 92
Pelló, R., et al. 2009, A&A, 508, 1173
Rosati, P., Borgani, S., & Norman, C. 2002, ARA&A, 40, 539
Rosati, P., et al. 2004, AJ, 127, 230
Rudnick, G., et al. 2009, ApJ, 700, 1559
Sawicki, M. 2002, AJ, 124, 3050
Simpson, C., & Eisenhardt, P. 1999, PASP, 111, 691
Simpson, C., et al. 2006, MNRAS, 372, 741
Spinrad, H., Dey, A., Stern, D., Dunlop, J., Peacock, J., Jimenez, R., & Windhorst, R. 1997, ApJ, 484, 581
Springel, V., et al. 2005, Nature, 435, 629
Stanford, S. A., Eisenhardt, P. R., & Dickinson, M. 1998, ApJ, 492, 461
Stanford, S. A., et al. 2005, ApJ, 634, L129
—. 2006, ApJ, 646, L13
Steidel, C. C., Adelberger, K. L., Shapley, A. E., Erb, D. K., Reddy, N. A., & Pettini, M. 2005, ApJ, 626, 44
Stern, D., Holden, B., Stanford, S. A., & Spinrad, H. 2003, AJ, 125, 2759
Tran, K., Franx, M., Illingworth, G. D., van Dokkum, P., Kelson, D. D., Blakeslee, J. P., & Postman, M. 2007, ApJ, 661, 750
van Breukelen, C., et al. 2007, MNRAS, 382, 971
—. 2009, MNRAS, 395, 11
van Dokkum, P. G., Franx, M., Fabricant, D., Illingworth, G. D., & Kelson, D. D. 2000, ApJ, 541, 95
van Dokkum, P. G., Franx, M., Kelson, D. D., & Illingworth, G. D. 1998a, ApJ, 504, L17+
van Dokkum, P. G., Franx, M., Kelson, D. D., Illingworth, G. D., Fisher, D., & Fabricant, D. 1998b, ApJ, 500, 714
van Dokkum, P. G., & van der Marel, R. P. 2007, ApJ, 655, 30
Venemans, B. P., et al. 2007, A&A, 461, 823
Visvanathan, N., & Sandage, A. 1977, ApJ, 216, 214
Williams, R. J., Quadri, R. F., Franx, M., van Dokkum, P., & Labbé, I. 2009, ApJ, 691, 1879
Wilson, G., et al. 2009, ApJ, 698, 1943
Yamada, T., et al. 2005, ApJ, 634, 861
Zirm, A. W., et al. 2008, ApJ, 680, 224